

Tomasz Poloczek, Waldemar Kwaśny, Artur Czupryński

The Effect of the Remelting and Laser Surface Alloying of Titanium Grade 5 (Ti6-Al-4V) on Erosive Wear Resistance

Abstract: The article presents the effect of the remelting and alloying of titanium grade 5 (Ti6-Al-4V) on erosive wear resistance (in accordance with the ASTM G76-04 standard). The study involved tests concerning the effect of graphite on the in-situ synthesis of titanium carbide during alloying performed using a Trudisk 3302 disk laser. The study also involved hardness measurements of individual beads as well as macro and microscopic tests. The tests involving the use of a Phenom World PRO scanning electron microscope provided with an EDS analyser as well as the X-ray phase analysis revealed the possible synthesis of titanium carbide during the laser alloying of the titanium surface with graphite. The erosive wear resistance of beads reinforced with composite particles was higher than that of the material in the as-received state, yet lower than that of the material remelted without the use of the alloying material.

Keywords: Remelting, Laser Surface Alloying, titanium grade 5, Ti6-Al-4V,

DOI: [10.17729/ebis.2022.2/3](https://doi.org/10.17729/ebis.2022.2/3)

Introduction

Because of their extremely high mechanical properties, resistance to the effect of various chemical environments and high strength-weight ratio, titanium alloys are widely applied in the aviation or automotive industries. Owing to the combination of light weight, resistance to temperature and a relatively insignificant decrease in mechanical properties along with an increase in temperature, the titanium alloy grade discussed in the article is used in the manufacturing of state-of-the-art aero-engine turbines exposed to the effect of sand and dust [1–5]. The process where solid particles cyclically strike the surface of a given material, leading to its removal, is referred to as erosion. The

aforesaid effect is highly important and desirable during sandblasting or waterjet cutting, yet in most cases the faster wear of materials as well as the degradation of their surface combined with increased surface roughness are unwanted phenomena. Because of potential failures of machinery elements, the issue of erosion continues to “enjoy” high popularity among researchers. S. Fidan [6], when investigating the effect of various conditions accompanying the heat treatment of alloy Ti6Al4V, discovered that ageing negatively affected erosion resistance. In turn, A. Lisiecki and A. Klimpel [7], using different shielding gases during laser remelting, increased the erosive wear resistance of various materials. Their solution involved

mgr inż. Tomasz Poloczek, dr hab. inż. Waldemar Kwaśny, dr inż. Artur Czupryński – Silesian University of Technology, Faculty of Mechanical Engineering; Department of Welding

the protection of the base material with argon and nitrogen-based gas shielding. T. Grögler [8], using chemical vapour diamond deposition on the titanium matrix, significantly increased erosive wear resistance (whereas physical gas phase-based deposition methods failed to provide desirable results). J. Zhou and S. Bahadur [9], when testing alloy Ti-6Al-4V within the temperature range of 200°C to 800°C, demonstrated that an increase in the material erosion rate grew along with an increase in temperature. The researchers also revealed the significant oxidation of the surface within the temperature range of 650°C to 800°C, thus proving the existence of the correlation between the titanium alloy erosion rate and surface corrosion resulting from the operational exposure of the material to higher temperature. Laser surface processing aimed to improve the erosive wear resistance of alloy Ti-6Al-4V continuous to be the subject of research, where Mo-WC [10], graphite-Si [11], SiC [12], NiCrBSi [13], NiCrBSi-TiC [14], Ti-Cr₃C₂ [15], NiCoCrAlY [16] and NiAl-ZrO₂ [17] are used as reinforcing phases. Surface processing plays an important role in technologies aimed to improve the operational properties of materials, enables the obtainment of significant savings resulting from the limited use of expensive materials as well as helps design elements characterised by appropriate surface properties and adapted for operation under specific environmental conditions. Laser surface alloying, being one of more popular surface processing methods, consists in the enrichment of the surface layer with alloying elements and/or the transformation of the material structure. Laser surface alloying techniques are the following [18]:

- single-stage process characterised by the continuous supply of the alloying material (in the form of powder) fed directly to the weld pool,

- dual-stage process, where the alloying material (in the form of paste – electrolytic coating) is applied on the substrate.

One of the popular variants of the alloying process used in relation to titanium alloys involves the use of the atmosphere of active gas where laser processing takes place (e.g. laser gas nitriding) [7].

The analysis of reference publications led to the conclusion that the graphite-based alloying of the titanium surface (aimed at the *in situ* formation of TiC-type carbide phases) could improve the erosive wear resistance of the above-named group of alloys.

Test materials and methods

The tests discussed in the article aimed to identify the effect of laser surface alloying and re-melting on the erosive wear resistance of one of the most popular titanium alloy grades on the market, i.e. Ti-6Al-4V (Grade 5). Before the tests, the specimens made of titanium grade 5 Ti-6Al-4V (having dimensions of 8 mm × 50 mm × 100 mm) were subjected to grinding followed by degreasing with ethanol. The purpose of the above-named procedures was to obtain the pure metallic surface as well as to improve the radiation absorptivity of the material subjected to alloying. In accordance with the manufacturer's (WOLFTEN) documentation, the material was made using the vacuum arc remelting process and, next, was subjected to hot rolling. The chemical composition of the base material and its mechanical properties are presented in Tables 1 and 2. The alloying process was performed using graphite powder (dispergated in ethanol) applied onto the surface subjected to laser processing before the commencement of the alloying process. The thickness of the layer applied amounted to approximately 200 µm.

Table 1. Chemical composition (% by weight) of the alloyed material (in the form of a plate made of Ti-6Al-4V) [24]

Al	V	Fe	O	C	N	Y	Ti
6.30	4.03	0.17	0.18	0.02	0.01	<0.0005	bal.

Table 2. Mechanical properties of the alloyed material (in the form of a plate made of Ti-6Al-4V) [24]

Hardness [HB]	Tensile strength R_m [MPa]	Yield point R_e [MPa]	Elongation [%]
335	1012	948	20

The structure of the base material used in the alloying tests is presented in Figure 1. The material represented the group of dual-phase titanium alloys, where the stabiliser of phase α is aluminium and that of phase β is vanadium.

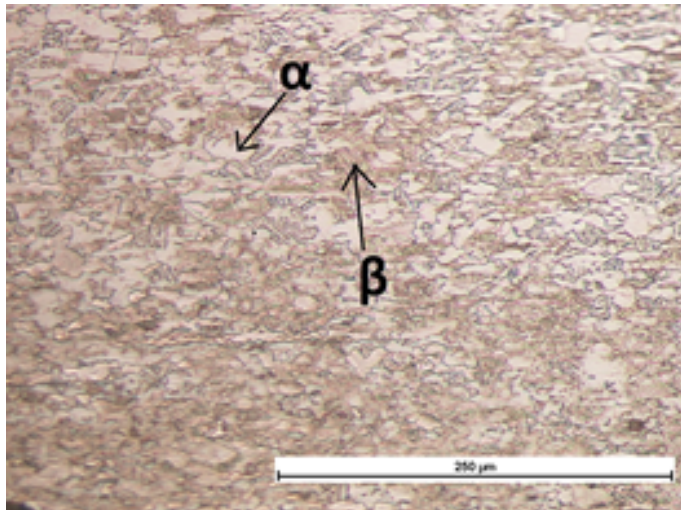


Fig. 1. Structure of the test material in the as-received state; etchant: Kroll's reagent

The laser alloying process was performed using a station equipped with a Trudisk 3302 disk laser (TRUMPF; Table 3) integrated with a numerically controlled system positioning the laser head in relation to the material subjected to processing. Based on initial remelting tests, to prevent the excessive penetration of the laser beam in the material and an increase in the surface area affected by the heat source, the laser beam focus (having a diameter of 200 μm) was located 35 mm above the surface of the material. The alloying process was shielded by Argon 5.0, fed through a cylindrical nozzle inclined at an angle of 30° in relation to the laser head.

Table 3. TRUMPF TruDisk 3302 laser parameters

Parameter	Value
Wavelength [μm]	1.03
Maximum beam power [W]	3300
Beam quality at the optical output [mm·rad]	<8.0
Optical fibre diameter [μm]	200
Focal length [mm]	200
Beam focus diameter [μm]	200
Optical fibre length [m]	20

The flow rate of the shielding gas amounted to 25 l/min. The performance of the initial tests enabled the development of optimum process parameters, i.e. a laser power of 1500 W, an alloying rate of 100 mm/min and a linear energy of 937 J/mm (Table 4).

The assessment of the quality of the coatings required the performance of macro and microscopic tests, conducted in accordance with the PN-EN ISO 17639 standard [21]. The macro and microscopic tests were performed using an Olympus SZX9 stereoscopic microscope and a Phenom World PRO scanning electron microscope provided with an EDS analyser. The specimens were etched (through immersion) in Kroll's reagent for 20 seconds. The XRD tests were performed using a PANalytical X'Pert PRO diffractometer equipped with a cobalt anode. Diffraction line profiles were obtained within the range of 2θ (between 25° and 130°), using the continuous scanning mode and a step of 0.1444°. The functional properties of the penetrations were assessed on the basis of results obtained in Vickers hardness tests (performed using a Wilson 401MVD Vickers hardness tester) as well as results obtained in erosive wear resistance tests. Microhardness tests (performed using a load of 200 g and an indenter penetration time of 12 seconds) were

Table 4. Alloying process parameters

Specimen no.	Graphite layer thickness [μm]	Laser power [W]	Remelting/alloying rate [mm/min]	Linear energy of the alloying process [J/mm]
1	-	1500	100	937
2	200	1500	100	937

carried out along three measurement lines, on the cross-section of each penetration (Fig. 2) (in accordance with the PN-EN ISO 6507 standard) [22]. Erosive wear resistance tests were performed in accordance with the ASTM G76-04 standard [25], using the Al_2O_3 erosive powder having an average grain size of 50 μm . The erosive particles were transported in the jet of dry air; the outlet velocity of the particles amounted to 70 m/s, whereas the flow rate of the erodent amounted to 2 g/min. The time, during which the erodent affected the specimen amounted to 10 minutes. The test was performed three times in relation to each specimen. The erodent angle of incidence amounted to 90° and 30° . The erosive loss mass (necessary to identify a related coefficient) was measured using a laboratory balance, with an accuracy of up to 0.0001 g.

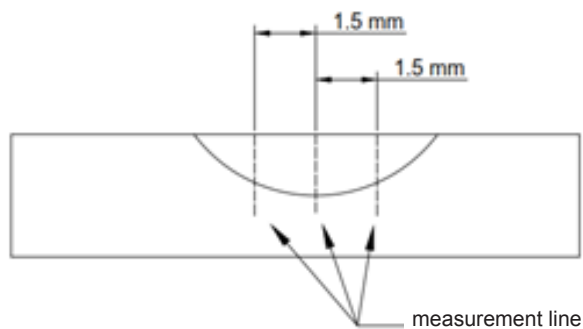


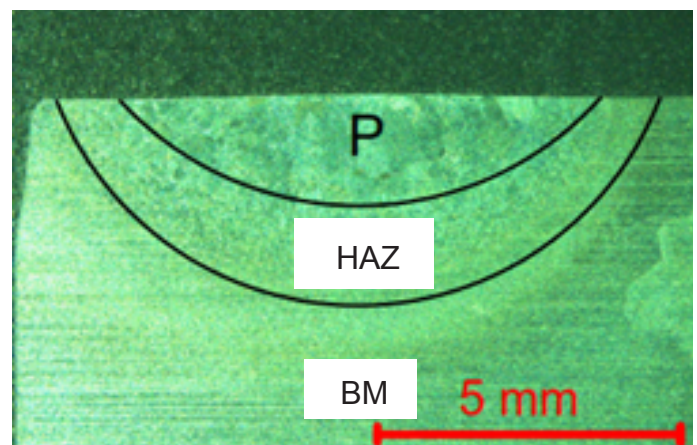
Fig. 2. Schematic diagram of the Vickers hardness test

Results

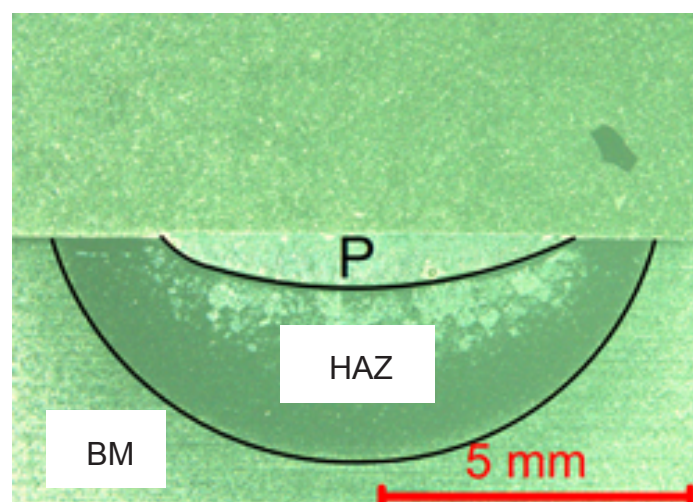
Photographs presenting the macrostructure of the laser alloyed beads are presented in Figure 3. Apart from a single pore located near the fusion line of specimen no. 2, the remaining specimens did not contain any welding imperfections, which indicated the proper adjustment of the process parameters. In terms of specimen no. 1, remelted without the use of the filler material, it was possible to observe significantly deeper penetration by the laser beam than that observed in specimen no. 2. The foregoing resulted from the use of the alloying material, which absorbed some energy and affected the intensity of convective movements in the liquid metal pool. It should be noted that the *in situ* reaction of TiC formation was the exothermic

reaction taking place between Ti and C in the liquid metal pool and, as such, generated additional energy. Calculations performed by D. Janicki [19] revealed that the amount of heat resulting from reactions occurring between Ti and C (in relation to the 15% content of TiC in the liquid metal pool) was relatively small (amounting between 10 J/mm and 20 J/mm). In comparison with the energy generated by the laser radiation source (i.e. 937 J/mm), the aforesaid energy was not significant and did not substantially affect the volume of the remelted material.

The microstructure of the bead remelted without the use of the alloying material contained acicular martensite α' and differed significantly from the material in the as-received state (containing the dual-phase $\alpha+\beta$



Specimen no. 1



Specimen no. 2

Fig. 3. Macrostructure of the material subjected to remelting (specimen no. 1) and to graphite-based alloying (specimen no. 2); etchant: Kroll's reagent

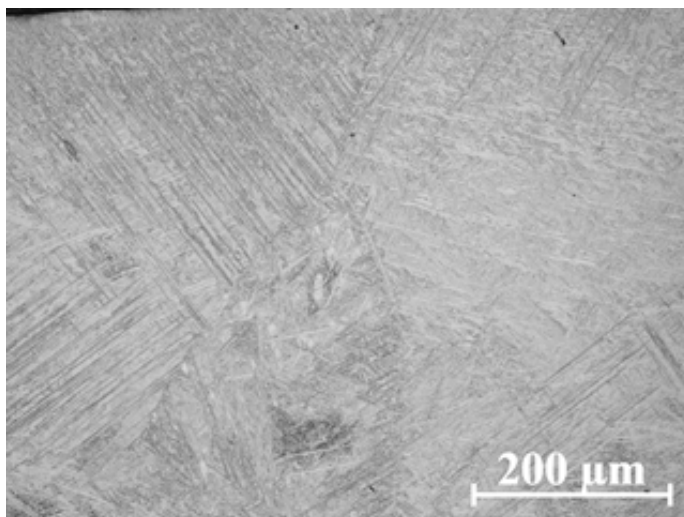


Fig. 4. Macrostructure of specimen no. 1 subjected to laser remelting; etchant: Kroll's reagent

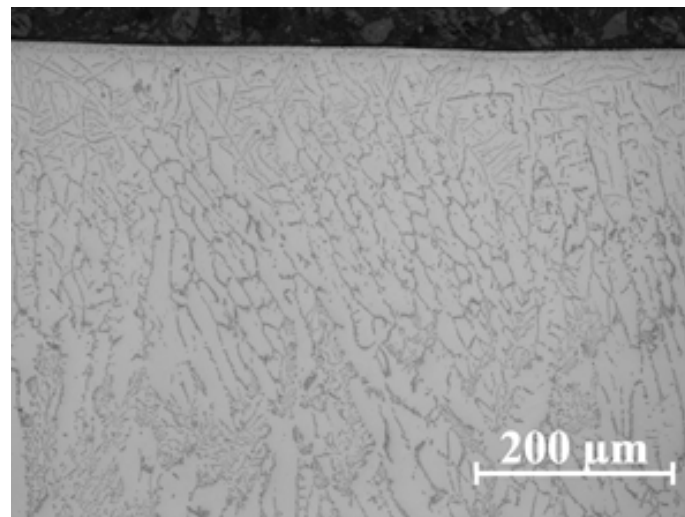
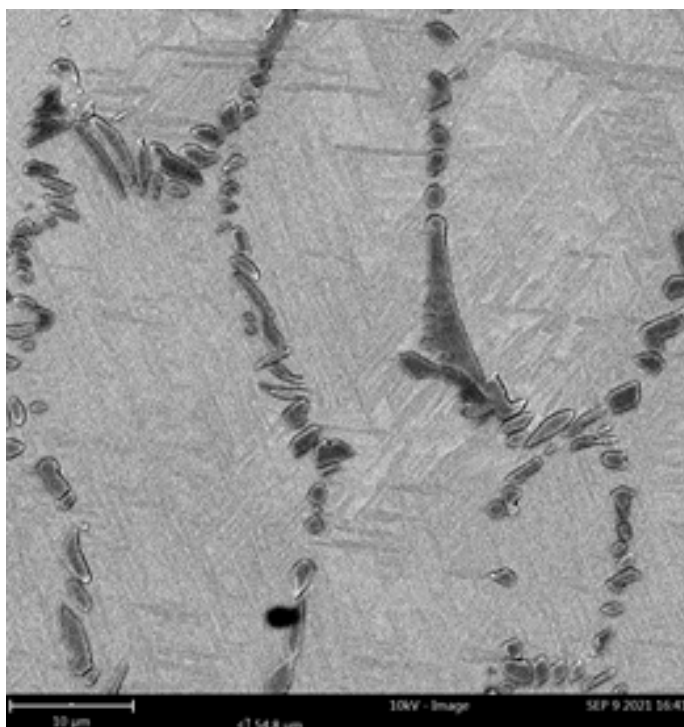


Fig. 5. Microstructure of specimen no. 2 subjected to graphite-based alloying; etchant –Kroll's reagent

structure). The foregoing resulted from high cooling rates accompanying the process of laser remelting (impeding diffusion between atoms) [23]. The martensite aciculae nucleated along the previous boundaries of grains β and were characterised by a high length-width ratio (Fig. 4).

The microstructure of specimen no. 2 contained easily visible precipitates of eutectic carbides (solidifying along grain boundaries) and the significantly smaller amount of primary carbides (Fig. 5). Based on the diagram

of the binary Ti-C phase system [20] it could be stated that, because of higher thermal stability than that of the alloy matrix, the titanium carbide solidified as the primary phase. The remaining carbide precipitates constituted the “strip” of the crystallisation of the grains of phase α' and, by preventing its growth, led to the formation of the fine-grained structure of the alloy. Figure 6 presents the eutectic structure of carbides, composed of small single TiC-type precipitates (also observed in the EDS microanalysis).



Chemical element symbol	Chemical element name	% by atoms	% by weight
Ti	titanium	56.30	83.70
C	carbon	43.70	16.30

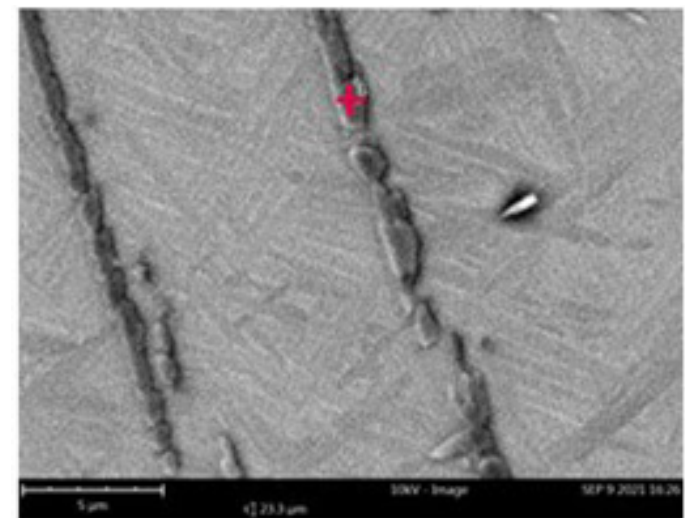


Fig. 6. Microstructure: a) morphology of the eutectic precipitates in specimen no. 2 and b) local EDS microanalysis of a precipitate in the structure of specimen no. 2

Radiographic analysis

The analysis of peaks obtained in the X-ray diffraction as well as the observations performed using the scanning electron microscope revealed *in situ* reactions taking place between graphite and titanium (during the laser surface alloying process). The diffraction indications revealed in the tests corresponded to the phases of α -Ti/ α' -Ti (HCP), β -Ti (BCC), TiC and C (Fig. 7). The material in the as-received state was characterised by reflections corresponding both to phase α -Ti and phase β -Ti. Specimen no. 1, subjected to argon-shielded remelting, was not characterised by the reflection observed in relation to a value of 2θ (amounting to 83°) (β -Ti). In turn, the remaining reflections, corresponding to phase β -Ti, overlapped with α -Ti/ α' -Ti, which, along with the results of the microstructural analysis, implied that the martensitic transformation of α' -Ti had taken place within the entire penetration. The carbon-related reflections observed in specimen no. 2 indicated that the alloying material (graphite) had not been entirely remelted in the liquid metal pool (carbon melting point being 3500°C), which, in turn, directly resulted from dynamic heating and cooling following the laser surface alloying process.

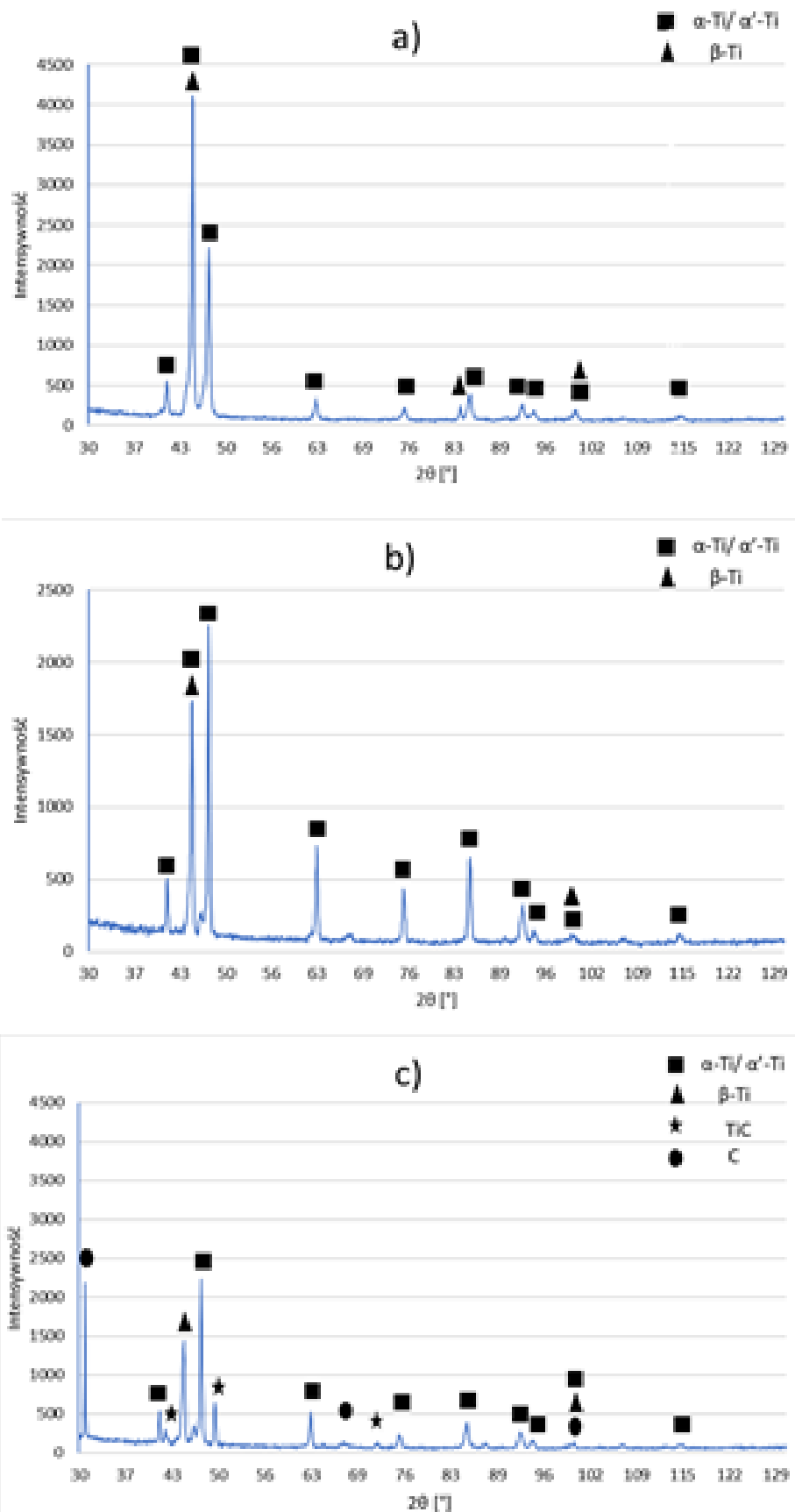


Fig. 7. Results of the XRD analysis: a) material in the as-received state, b) specimen no. 1 and c) specimen no. 2

Hardness measurements

The analysis of the cross-sectional hardness distribution made it possible to distinguish the three primary zones of the joint, i.e. the area of penetration, the heat affected zone and the base material (whose average hardness amounted to 340 HV_{0.3}). The bead alloyed using graphite (specimen no. 2) was characterised by a significant increase in hardness (the average hardness value amounted to 410 HV_{0.3}). The significant value of standard deviation in relation to specimen no. 2 resulted from the non-homogeneity of its structure and the resultant difference between carbides and their matrix composed of titanium. The hardness measurements revealed that the parameters applied in the alloying process triggered the martensitic transformation in the fusion zone (having a hardness of approximately 380 HV_{0.3} (specimen no. 1) and, partly, in the heat affected zone (having a hardness of approximately 370 HV_{0.3} (Fig. 8)).

Erosive wear resistance tests

Figure 9 contains a diagram presenting the erosion-triggered material loss (identified in accordance with the procedure specified in the ASTM G76-04 standard [25]). The analysis involved the material in the as-received state as well as the remelted and alloyed beads subjected to laser processing. The tests revealed that mass losses (in each case) were greater in relation to an erodent angle of incidence of 30°. The most favourable erosive wear resistance was observed in relation to specimen no. 1, subjected to remelting without the use of the alloying

material. The mass loss concerning the above-named specimen was nearly by twice lower than that of the material in the as-received state. The foregoing resulted from the laser remelting-triggered martensitic transformation of the structure, enabling the crystallisation of phase α' (characterised by high hardness). The erosive wear mechanism observed in relation to the martensitic structure of the titanium alloy was typical of plastic materials, where the erosion-triggered loss of material resulted from the micro-cutting of the plastic matrix (which was demonstrated in the SEM photographs of the beads subjected to the erosive wear tests (Fig. 10)). In terms of specimen no. 2, containing reinforcing phases in the form of

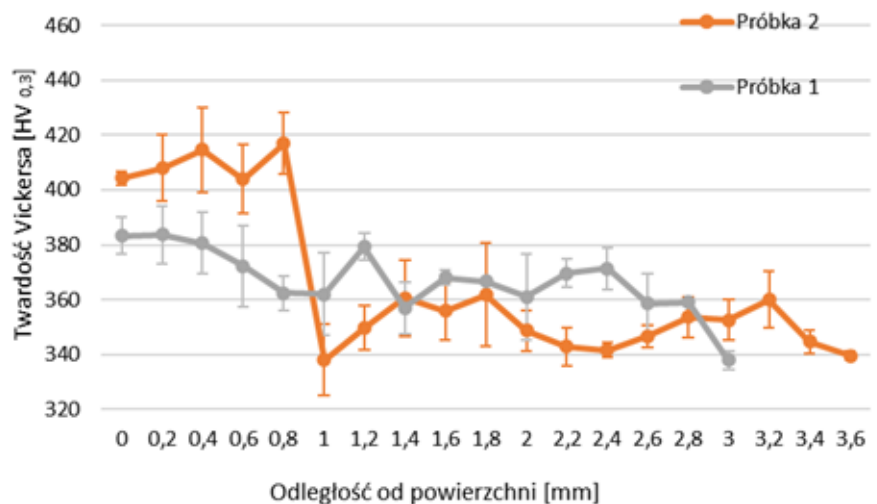


Fig. 8. Hardness measurement results

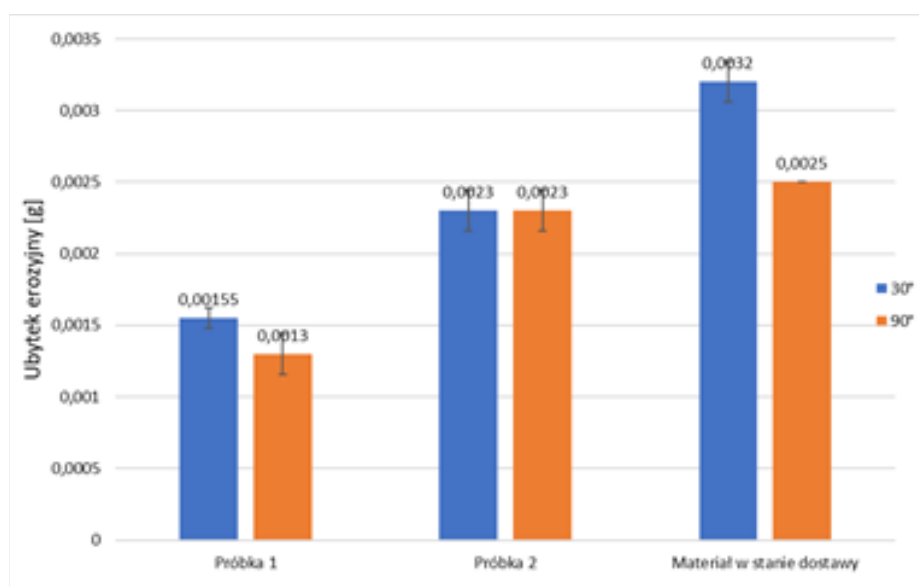
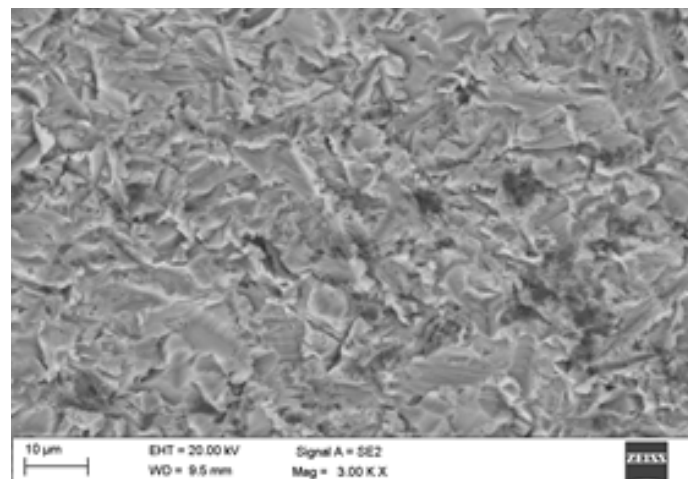
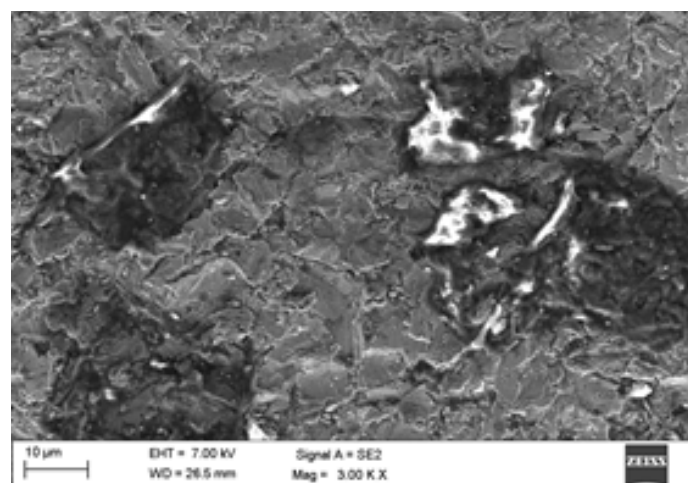


Fig. 9. Value of the erosion-triggered loss of mass in the test materials in relation to the erodent angle of incidence

titanium carbides (TiC), the losses of mass were greater than those observed in specimen no. 1. The aforesaid losses were the consequence of the erosive wear mechanism. As regards specimen no. 2, the making of which involved the use of graphite (used to obtain hard TiC-based reinforcing phases), the material affected by erodent particles revealed the simultaneous occurrence of two erosive wear mechanisms. The first mechanism, typical of plastic materials, was responsible for the loss of the matrix material, whereas the second one led to the cracking and, next, the chipping of the hard particles of the TiC-based reinforcing phase. It was also observed that the contribution of each of the above-named mechanisms to the erosive wear process was independent of the erodent angle of incidence (which was demonstrated in the diagram presented in Fig. 9).



Specimen no. 1



Specimen no. 2

Fig. 10. Photographs (SEM) of craters observed after the erosive wear tests

Conclusions

The above-presented tests and their results justified the formulation of the following conclusions:

- The laser surface alloying process involved the reaction between graphite and the base material (Ti6Al4V), enabling the in situ synthesis of titanium carbide.
- The results of the microscopic tests revealed the possibility of obtaining structures characterised by the highly uniform distribution of the reinforcing phase (TiC) in the metallic matrix of the alloy.
- The processing of the surface performed using the disk laser was characterised by high cooling rates, thus triggering (during cooling) the transformation of phase β -Ti into acicular martensite α' (characterised by a hardness of up to 380 HV_{0.3}). The average micro-hardness of the composite TiC-reinforced composite beads was by approximately 20% higher (410 HV_{0.2}) than that of the material in the as-received state.
- The erosive wear resistance of the composite beads reinforced with composite particles was by approximately 20% higher than that of the material in the as-received state, yet by approximately 39% lower than that of the material remelted without the use of the alloying material.
- The TiC-based reinforcing phase affected the nature of the erosive wear mechanism, which combined the typical wear of the matrix triggered by micro-cutting and ridging processes as well as the crumbling and the chipping of the hard TiC particles off the eroded surface.
- The laser remelting of the surface of alloy Ti6Al4V led to the obtainment of the highest erosive wear properties, resulting from the homogenous structure composed of acicular lamellas (characterised by a relatively high hardness of 380 HV_{0.3}).

The publication received support within the programme Excellence Initiative – Research University, implemented at the Silesian University of Technology in 2021.

References

- [1] Manhabosco T., Tamborim S., Santos C., Müller I.: Tribological, electrochemical and tribo-electrochemical characterization of bare and nitrided Ti6Al4V in simulated body fluid solution. *Corrosion Science*, 2011, no. 53, pp. 1786–1793.
- [2] Li J., Sun M., Ma X., Tang G.: Structure and tribological performance of modified layer on Ti6Al4V alloy by plasma-based ion implantation with oxygen. *Wear*, 2006, vol. 261, no. 11–12, pp. 1247–1252.
- [3] Martini C., Ceschini L.: A comparative study of the tribological behaviour of PVD coatings on the Ti–6Al–4V alloy. *Tribology International*, 2011, vol. 44, no. 3, pp. 297–308.
- [4] Yetim A., Celik A., Alasaran A.: Improving tribological properties of Ti6Al4V alloy with duplex surface treatment. *Surface Coating Technology*, 2010, vol. 205, no. 2, pp. 320–324.
- [5] Yetim A., Yildiz F., Vangolu Y., Alasaran A., Celik A.: Several plasma diffusion processes for improving wear properties of Ti6Al4V alloy. *Wear*, 2009, vol. 267, no. 12, pp. 2179–2185.
- [6] Fidan S., Avcu E., Karakulak E., Yamanoğlu R., Zeren M., Sinmazcelik T.: Effect of heat treatment on erosive wear behaviour of Ti6Al4V alloy. *Materials Science and Technology*, 2013, vol. 29, no. 9, pp. 1088–1094.
- [7] Lisiecki A., Klimpel A.: Diode laser surface modification of Ti6Al4V alloy to improve erosion wear resistance. *Archives of Materials Science and Engineering*, 2008, vol. 32, no. 1, pp. 5–12.
- [8] Grögler T., Zeiler E., Franz A., Plewa O., Rosiwal S., Singer R.: Erosion resistance of CVD diamond-coated titanium alloy for aerospace applications. *Surface & Coatings Technology*, 1999, no. 112, pp. 129–132.
- [9] Zhou J.R., Bahadur S.: Erosion-corrosion of Ti-6Al-4V in elevated temperature air environment. *Wear*, 1995, vol. 186–187, no. 1, pp. 332–339.
- [10] Pang W., Man H., Yue T.: Laser surface coating of Mo–WC metal matrix composite on Ti6Al4V alloy. *Materials Science and Engineering: A*, 2005, vol. 390, no. 1–2, pp. 144–153.
- [11] Tian Y.S., Chen C.Z., Chen L.X., Huo Q.H.: Microstructures and wear properties of composite coatings produced by laser alloying of Ti-6Al-4V with graphite and silicon mixed powders. *Materials Letters*, 2006, vol. 60, no. 1, pp. 109–113.
- [12] Selamat M.S., Watson L.M., Baker T.N.: XRD and XPS studies on surface MMC layer of SiC reinforced Ti-6Al-4V alloy. *Journal of Materials Processing Technology*, 2003, vol. 142, no. 3, pp. 725–737.
- [13] Sun R.L., Yang D.Z., Guo L.X., Dong S.L.: Microstructure and wear resistance of NiCrBSi laser clad layer on titanium alloy substrate. *Surface and Coatings Technology*, 2000, vol. 132, no. 2–3, pp. 251–255.
- [14] Sun R.L., Yang D.Z., Guo L.X., Dong S.L.: Laser cladding of Ti-6Al-4V alloy with TiC and TiC+NiCrBSi powders. *Surface and Coatings Technology*, 2001, vol. 135, no. 2–3, pp. 307–312.
- [15] Zhang S., Wu W.T., Wang M.C., Man H.C.: In-situ synthesis and wear performance of TiC particle reinforced composite coating on alloy Ti6Al4V. *Surface and Coatings Technology*, 2001, vol. 138, no. 1, pp. 95–100.
- [16] Meng Q., Geng L., Ni D.: Laser cladding NiCoCrAlY coating on Ti-6Al-4V. *Materials Letters*, 2005, vol. 59, no. 22, pp. 2774–2777.
- [17] Sha C.K., Lin J.C., Tsai H.L.: The impact characteristics of Ti-6Al-4V plates

- hardfacing by laser alloying NiAl+ZrO₂ powder. *Journal of Materials Processing Technology*, 2003, vol. 140, no. 1–3, pp. 197–202.
- [18] Dobrzański L.A., Tański T., Dobrzańska-Danikiewicz A., Król M., Malara S., Domagała-Dubiel J.: *Struktura i własności stopów Mg-Al-Zn*. International OCSCO World Press, Gliwice 2012.
- [19] Janicki D.: Effect of Chromium and Molybdenum Addition on the Microstructure of In Situ TiC-Reinforced Composite Surface Layers Fabricated on Ductile Cast Iron by Laser Alloying. *Materials*, 2020, vol. 13, no. 24.
- [20] Bandyopadhyay D., Sharma R.C., Chakraborti N.: The Ti-Co-C System (Titanium – Cobalt – Carbon). *Journal of Phase Equilibria*, 2020, vol. 21, no. 2, pp. 79–185.
- [21] PN-EN ISO 17639. *Badania niszczące spawanych złączy metali -- Badania makroskopowe i mikroskopowe złączy spawanych*.
- [22] Norma: PN-EN ISO 6507. *Metale -- Pomiar twardości sposobem Vickersa*.
- [23] Vrancken B., Thijs L., Kruth J.P., Humbeeck J.V.: Microstructure and mechanical properties of a novel β titanium metallic composite by selective laser melting. *Acta Materialia*, 2014, vol. 68, no. 15, pp. 50–158.
- [24] ATI Speciality Materials – Test certificate no. 121626, 09.08.2017.
- [25] ASTM G76-04:2004. *Standard test method for conducting erosion tests by solid particle impingement using gas jets*.